11-1-2022

The Impact of Biofilms and Dissolved Organic Matter on the Transport of Nanoparticles in Field-Scale Streams

Junyeol Kim
University of Notre Dame

Kevin R. Roche
Boise State University

Diogo Bolster
University of Notre Dame

Kyle Doudrick
University of Notre Dame

Publication Information

Kim, Junyeol; Roche, Kevin R.; Bolster, Diogo; and Doudrick, Kyle. (2022). "The Impact of Biofilms and Dissolved Organic Matter on the Transport of Nanoparticles in Field-Scale Streams". *Water Research, 226*, 119206. https://doi.org/10.1016/j.watres.2022.119206

The Impact of Biofilms and Dissolved Organic Matter on the Transport of Nanoparticles in Field-Scale Streams

Authors:

Junyeol Kim[a], Kevin Roche[b], Diogo Bolster[a], Kyle Doudrick[a*]

Affiliations:

[a]Department of Civil and Environmental Engineering and Earth Sciences, University of Notre Dame, Notre Dame, IN 46556

[b]Department of Civil Engineering, Boise State University, Boise, ID, 83725

[*]**Corresponding Authors and Address:**

Kyle Doudrick, Department of Civil and Environmental Engineering and Earth Sciences, University of Notre Dame, Notre Dame, Indiana, USA, 46637

Phone: 5746310305

e-mail: kdoudrick@nd.edu

JOURNAL: Water Research

Date: September 18, 2022

Abstract

The fate and transport of nanoparticles (NPs) in streams is critical for understanding their overall environmental impact. Using a unique field-scale stream at the Notre Dame-Linked Experimental Ecosystem Facility, we investigated the impact of biofilms and the presence of dissolved organic matter (DOM) on the transport of titanium dioxide (TiO_2) NPs. Experimental breakthrough curves were analyzed using temporal moments and fit using a mobile-immobile model. The presence of biofilms in the stream severely reduced the transport of the TiO_2 NPs, but this was mitigated by the presence of DOM. Under minimal biofilm conditions, the presence of DOM increased the mass recovery of TiO_2 from 4.2% to 32% for samples taken 50 m downstream. For thriving biofilm conditions only 0.5% of the TiO_2 mass was recovered (50 m), but the presence of DOM improved the mass recovery TiO_2 to 36%. The model was suitable for predicting early, peak, tail, and truncation time portions of the breakthrough curves, which attests to its ability to capture a range of processes in the mobile and immobile domains of the stream. The model outcomes supported the hypothesis that DOM changed the interaction of NP-biofilm interaction from an irreversible to a reversible process. Collectively, these outcomes stress the importance of considering biogeological complexity when predicting the transport of NPs in streams.

47

48 **Keywords:** Nanoparticles; titanium dioxide; fate and transport; streams; field-scale; mobile-

49 immobile; biofilms, dissolved organic matter

1.0 INTRODUCTION

Engineered nanoparticles (NPs) are widely used in consumer, industrial, agricultural, and pharmaceutical products (Fei Yin et al., 2013; Pan and Xing, 2012; Volder et al., 2013; Zhang et al., 2013). During their life cycle, NPs can enter streams through various pathways [e.g., wastewater treatment plants (Choi et al., 2017; Westerhoff et al., 2011)], and streams are efficient transport networks that can potentially move the NPs throughout the environment. Thus, proper risk assessment of NPs requires an understanding of their fate and transport in streams. This has proven difficult due to the complexity arising from a combination of enumerable stream biogeochemical conditions and realistic NP physical-chemical properties that are difficult to measure in the environment.

NP transport in streams is typically simplified at the lab-scale using batch or column reactors to simulate NP behavior in the water column or the porous media of the streambed, respectively (Darlington et al., 2009; Wang et al., 2016) . While these experiments are valuable for understanding specific mechanisms (e.g., homoaggregation) as a function of various parameters (e.g., pH), field-scale transport studies are a necessary step for ultimately understanding transport in realistic systems. As depicted in Figure 1, streams are complex, reactive systems with rapid, turbulent flows in the water column (mobile domain) connected to slower flows in the streambed substrate (relatively immobile domain) (Newbold et al., 2005). As NPs move downstream, they can aggregate, settle, and deposit at the water-streambed interface or be driven into the streambed via advective hyporheic exchange. Through hyporheic exchange, NPs can be temporarily retained in the streambed or entirely removed via physical storage (Newbold et al., 2005) or hyporheic/benthic biofilms (Arnon et al., 2010; Battin et al., 2003; Roche et al., 2017). NPs that are not irreversibly deposited in the streambed or biological media will be

resuspended and arrive downstream at an orders of magnitude longer timescale than NPs moving through the water column only.

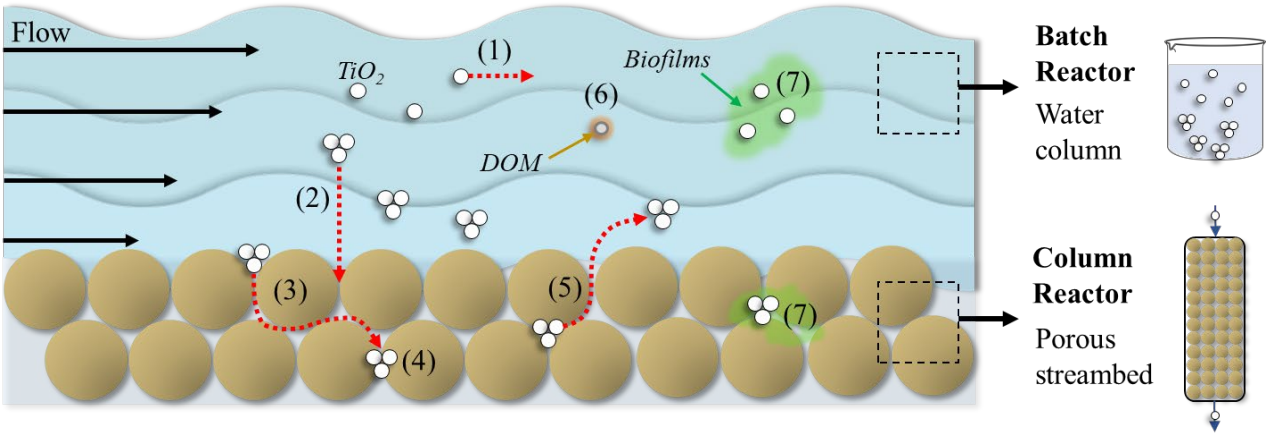

Figure 1. (a) Conceptual diagram of NP transport in streams with connection process typically described using laboratory experiments. (1) NPs move through the water column (mobile domain), where they can undergo (2) aggregation and settle to the interface between the water column and streambed substrates (immobile domain). (3) Hyporheic exchange drives NPs at the interface into the streambed where they can be (4) permanently retained or (5) resuspended to the water column. NPs can (6) interact with dissolved organic matter (DOM) that can stabilize and enhance transport, or they can (7) become retained in biological media that is present in the mobile and immobile domains. Other NP reactions such as dissolution or transformation (e.g., sulfidation) can occur but are not expected to dominate transport for most NP types. At the lab-scale, batch reactors studies are used to predict NP behavior in the water column or pore space of the streambed, while column studies are used to predict NP behavior in the porous streambed substrate. The transport of NPs in the streams is controlled by exchanges between the water column and streambed, as well as interactions between NPs and biogeological media, and the complexity cannot be fully captured with the lab-scale batch and column studies depicted.

Prior studies on the transport behavior of (ultra)fine particles in streams have mostly involved naturally occurring particles such as clays, silts, particulate organic matter, microbes, and metal oxides (Areepitak and Ren, 2011; Arnon et al., 2010; Drummond et al., 2014b, 2014a; Minshall et al., 2000; Packman et al., 2000; Ren and Packman, 2005). From strictly a size perspective, finite differences are expected between engineered NPs and naturally occurring ultrafine particles that have a nominal diameter less than 1 μm. But potential transport behavior variations could arise between the two due to the unique physical-chemical properties of engineered NPs. Studies focused on the transport of NPs in streams have been mostly limited to controlled laboratory experiments (Battin et al., 2009; Boncagni et al., 2009), with only a few studies using realistic field-scale experiments (Kim et al., 2019). Boncagni et al. investigated the transport of titanium dioxide (TiO_2) NPs using flume, column, and batch laboratory experiments (Boncagni et al., 2009). They observed the NPs to aggregate in the water column and deposit in the streambed, with both streambed velocity and pH playing a critical role in the detachment and resuspension of the NPs into the stream. Two different engineered TiO_2 NPs were used, yet their transport behavior was dissimilar due to differences in their surface chemistry. Battin et al. investigated the effect of biofilms on the transport of two TiO_2 NPs in a laboratory column (Battin et al., 2009). The transport behavior was heavily influenced by the presence of biofilms, with downstream travel distances reduced approximately two and a half fold. This agreed with outcomes for naturally occurring particulates (Battin et al., 2008), but again, notable differences were observed for the two TiO_2 NPs, suggesting their specific engineered surface chemistry affected the biogeochemical interactions. Kim et al. conducted a controlled field-stream release transport study for catalytic- and food-grade TiO_2 NPs (Kim et al., 2019). The streambed media

size, presence of biofilms, and surface properties of the NPs had a marked effect on the transport behavior. The mass loss of the TiO_2 NPs in the stream increased with increasing streambed particle size, reflecting an increased rate in hyporheic exchange and subsequent retention in the streambed via attachment. The TiO_2 mass loss was exacerbated in the presence of biofilms in the water column and immobile streambed. When negatively charge food-grade TiO_2 NPs were used, the mass recovery increased for all conditions tested compared to the bare catalytic-grade TiO_2 NPs, which highlights the importance of the NP surface charge on transport under realistic stream conditions.

The presence of dissolved organic matter (DOM) in streams can have a marked effect on the transport of NPs, yet thus far studies been limited to controlled laboratory bench-scale experiments. In aqueous systems, DOM stabilizes NPs and enhances transport (Domingos et al., 2009; Isaacson and Bouchard, 2010; Li and Chen, 2012; Nason et al., 2012; Stankus et al., 2011; Thio et al., 2011; Vindedahl et al., 2016; Zhang et al., 2009; Zhu et al., 2014), but DOM may also alter the surface charge of the porous streambed media and increase NP retention (Zhou and Cheng, 2018). This contrasting behavior highlights the importance for exploring realistic stream systems that contain both water column and streambed domains.

Thus, the goal of this study was to investigate the impact of biofilms and DOM on the transport of NPs in field-scale streams. The stream experiments were conducted at the Notre Dame-Linked Experimental Ecosystem Facility (ND-LEEF) in a 55 m reach lined with mixed-sized streambed substrate. Experiments were conducted in the spring and autumn when biofilms were minimal and thriving in the streams, respectively. TiO_2 NPs were chosen as a model NP due to their widespread use as a whitening agent and ultraviolet light absorbing material in a variety of consumer products (Allen et al., 2002; El-Sherbiny et al., 2014; Gondikas et al., 2014; Johnson et

al., 2011; Keller et al., 2014; Shi et al., 2013). The results of this study are also applicable to a range of ultrafine particles for which no information currently exists at field-scale, regarding the effect of biofilms and DOM. The transport breakthrough curves were modeled with a mobile-immobile model (MIM) that can capture the commonly observed range of processes relevant to transport in complex environmental systems, including heavy tails in breakthrough curves and non-exponential retention and reaction processes (Aubeneau et al., 2014; Bolster et al., 2019). The MIM has been successfully used to predict biological and geological particle transport in field-scale streams (Aubeneau et al., 2016, 2015a, 2015b, 2014; Boano et al., 2007; Drummond et al., 2014), and we have shown it to be an excellent framework for capturing conservative and reactive transport at ND-LEEF in experiments with very strong anomalous transport characteristics (Roche et al., 2019a).

2.0 MATERIALS AND METHODS

2.1 Materials

A commercial catalytic-grade TiO_2 NP called P90 was used as a model NP (donated by Evonik, Essen, Germany)). P90 is a mixed-phase TiO_2 consisting of anatase (~85%) and rutile (~15%) with an average primary particle size of approximately 12 and 18 nm, respectively (Kim and Doudrick, 2019). The point of zero charge (pH_{zpc}) of P90 in water as measured by zeta potential analysis is approximately 6.0 (Kim and Doudrick, 2019). Unless specified otherwise, all chemical solutions used in this study were prepared with ultrapure water (18.2 MΩ-cm) produced using a Barnstead Nanopure treatment system (Thermo-Fisher Scientific). Rhodamine water tracer (RWT; $C_{29}H_{29}ClN_2Na_2O_5$; Acros Organics, NJ, USA) was used as a conservative solute in the stream experiments and has been previously shown to be a suitable tracer at our field-site (Aubeneau et al., 2016, 2015a, 2015b, 2014; Shogren et al., 2017). The RWT solutions were covered with

aluminum foil to prevent any photolytic degradation prior to release. The DOM was extracted from commercial topsoil that contained no fertilizer (Premium Topsoil, Model #71130758, Scotts, OH, USA). To prepare the DOM solution, the topsoil was first dispersed in ultrapure water, mixed for 30 min, and then allowed to settle for 30 min. Then, the top solution was centrifuged at 8000×g for 10 min and the supernatant was passed through a 0.45 μm filter (Nylon, Whatman®). The filtrate DOM was stored in an amber bottle at 4 °C for later use and analysis. The DOM extract was diluted 20x, and the $SUVA_{254}$ was analyzed using a UV-Vis spectrometer (DR6000, HACH, Loveland, CO, USA). Total organic carbon (TOC) was measured using a TOC analyzer (TOC-L, Shimadzu, Columbia, MD, USA) (Potter and Wimsatt, 2005). The TOC of the DOM solution after dilution was 10.5 mgC L^{-1}, and the $SUVA_{254}$ was 5.6 L mgC^{-1} m^{-1}, which suggests high aromaticity of ~40% (Weishaar et al., 2003).

2.2 Hydrodynamic Size and Zeta Potential of NPs in Stream Water

The homoaggregation behavior of TiO_2 NPs was characterized using dynamic light scattering (DLS) and phase analysis light scattering (PALS) (NanoBrook Omni, Brookhaven Instrument Corporation, Holtsville, NY). DLS was used to measure the hydrodynamic diameter and PALS was used to measure the zeta potential (ζ). Analyses were conducted in ultrapure water (pH 5.2) and stream water (pH 8.1) for bare TiO_2 NPs and TiO_2 NPs mixed with DOM (TiO_2-DOM).

For DLS, TiO_2 powder was added to the target liquid medium (i.e., ultrapure or stream water) to achieve a concentration of 10 mg L^{-1}. TiO_2-DOM was prepared similarly but in the presence 5 mgC L^{-1} of DOM. The samples were immediately analyzed after vigorously shaking the solutions for 5 s. Note, when TiO_2 NP powder is added to water it rapidly aggregates and it can take multiple hours of mixing or sonication to disperse the NPs. As such, the DLS results are

used herein to characterize the general homoaggregation behavior as a comparative function of water medium (e.g., stream, ultrapure, presence of DOM), and they are not expected to accurately predict the size of the NPs during the stream experiments.

The preparation of samples for zeta potential analysis was identical to DLS, but TiO_2 solutions were prepared at a concentration of 100 μg L^{-1}. 1 mM KNO_3 was used as a supporting electrolyte for ultrapure water and no electrolyte was added to the stream water due to the already existing conductivity. Thirty measurement cycles were conducted at 25 °C in triplicate, and the average and standard errors are reported. The Smoluchowski model (i.e., $\kappa a > 1$, $f = 1$) was used to calculate the zeta potential from electrophoretic mobility (Lowry et al., 2016).

2.3 Stream Experiments

All field stream experiments were conducted at ND-LEEF located at St. Patrick's County Park in South Bend, IN, USA (Figure 2A). ND-LEEF is a globally unique research facility that at the time of the experiments contained two man-made experimental watersheds, each consisting of an interconnected pond, two stream reaches (4 streams total), and a wetland. Each stream is 0.4 m wide and 55 m long with a hydraulic gradient of 0.0075. The volume of streambed substrate is approximately 3,675 L. The stream channel base is lined with cement concrete to prevent unwanted interactions with the surrounding environment. The streambed is lined with a 1:1:1 volume ratio of sand, pea gravel, and cobble stone with a D_{50} size of 0.053, 0.67, and 5 cm, respectively. The streambed media is approximately 10 cm thick. Prior to turning on the water for the experimental season, the streams were biologically "reset" by removing terrestrial organic matter (e.g., leaves, sticks) and benthic biofilms by hand. The top layer of the streambed (~2-5 cm) was physically mixed to mobilize and remove any remaining organic matter. The substrate was then graded to a mostly flat topography with natural roughness features.

208 The stream system is normally fed through a constant-head reservoir supplied by
209 groundwater (not shown in Figure 2A). The average hydraulic residence time in the reservoir is
210 about 3.5 days before reaching the streams. The water flows from the upper streams into two
211 ponds, which then feed into the lower streams. Typically, at the start of the experimental season
212 (~May), the flow from the reservoir is set and all streams receive this water constantly until the
213 end of the season (~Nov.). The groundwater that feeds the streams is very hard with high ionic
214 strength (19 mM on average) and conductivity (507 µS on average), which can cause severe NP
215 aggregation (Kim et al., 2019). Thus, to minimize NP aggregation in this study, all experiments
216 were conducted with the feed from the groundwater reservoir turned off and a separate pump was
217 used to deliver water directly from the pond to the head of the stream (0.88 L/s). The pond water
218 consisted of groundwater from the previous season and rainwater accumulated while the reservoir
219 pump was turned off. The stream experiments were conducted two times during the year: first in
220 June, when the biofilm growth was minimal (Figure 2B and Figure S1), and then in September
221 after biofilms were flourishing in the stream (Figure 2C).
222
223

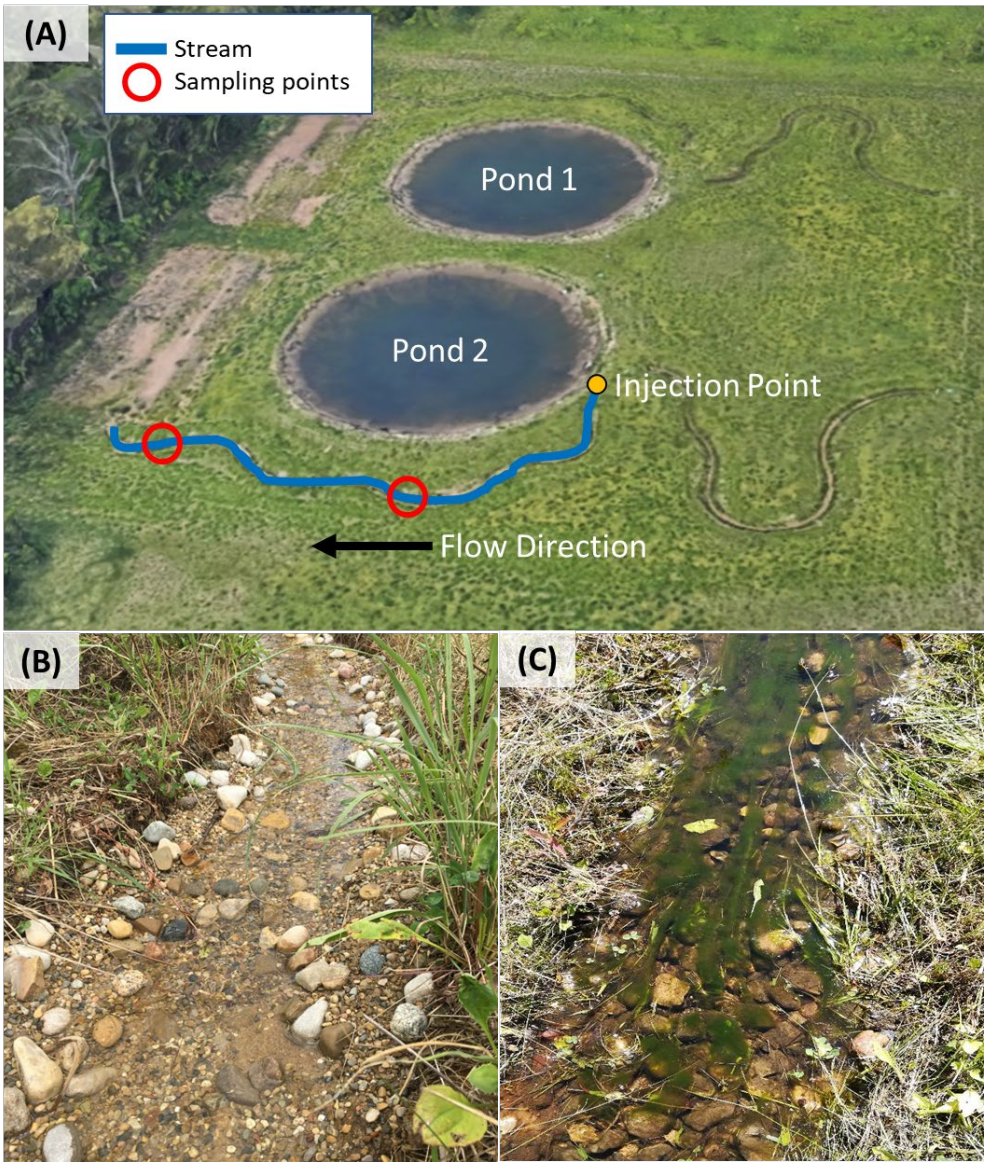

Figure 2. (A) Aerial photograph (Google Earth) of the ND-LEEF site with schematics detailing the stream location and the 25- and 50-m sampling points. Photographs of the stream during (B) minimal biofilm conditions in June and (C) thriving biofilm conditions in September.

Before each stream release event, the pH, temperature, and conductivity were measured on-site. Samples were also taken for off-site analyses, including total suspended solids (TSS), total dissolved solids (TDS), chlorophyll a (Chl a), ash-free dry mass (AFDM), and the background Ti

concentration. A modified ESS 150.1 method (EPA, 1991) and the top-rock scrape sampling method (Berkman and Canova, 2007) were used for the analysis of Chl a and AFDM, respectively. Detailed methods for stream water characterization are available in the Supplementary Materials.

All stream experiments were conducted using a short-term pulse injection of 1 L solutions. Each stream release scenario consisted of three separate experiments: RWT, TiO_2, and TiO_2-DOM. The mass of the RWT was 121 and 400 mg injected in June and September, respectively. The mass of the TiO_2 NPs injected was 4 g for all experiments. These concentrations were chosen based on prior knowledge about the mass required to maximize the separation between the peak and tail of the breakthrough curves, which was controlled by the detection limits of the respective analyses (Section 2.4). This was necessary to obtain enough data to properly develop the numerical models. RWT and TiO_2 solutions (or suspensions) were prepared in the lab immediately before traveling to the field site. Each solution was vigorously mixed for approximately 10 min before the pulse addition. For the injection, the 1-L solution was rapidly poured into the stream at the head (i.e., 0-m point). For the TiO_2-DOM experiment, TiO_2 and DOM solutions were not pre-mixed. Rather, the 1-L suspension of TiO_2 (4 g L^{-1}) was co-released with a 1-L solution of DOM (~210 mgC L^{-1}). Immediately upon injection, a timer was started, and periodic water column samples were collected at a stream depth approximately halfway to the streambed using 50 mL tubes (Polypropylene, Sterile, VWR, Batavia, IL). This was done at points 25 and 50 m downstream. Each experiment was conducted one time. Immediately after completing the transport experiment, biofilms were collected for later Ti analysis (detailed methods available in the Supplementary Materials).

To avoid cross-contamination between TiO_2 and TiO_2-DOM, field experiments were conducted 48 hrs apart. Background Ti analyses confirmed no TiO_2 existed in the water prior to

each experiment, though the possibility of TiO_2 stored in the streambed is justified. Considering the volume (~3,675 L) and surface area of streambed substrates are much greater than the amount of TiO_2 used in each experiment, the influence from prior experiments is expected to be minimal.

2.4 Quantification of Conservative Tracers and Nanoparticles

RWT concentrations were analyzed using a handheld fluorometer (DataBank™, Turner Designs Inc., San Jose, USA) equipped with a Cyclops sensor (Cyclops-7F, Turner Designs Inc.). The sensor was calibrated in the lab under dark conditions. At the 50-m sampling point, the sensor was placed parallelly to the streambed and was covered with a cardboard box to prevent interferences from the sunlight. The concentration of RWT was measured every 2 seconds. At the 25-m sampling point, samples were collected periodically, stored in the dark, and then the concentration of RWT was measured in the lab.

TiO_2 samples collected at 25 and 50 m were quantified using a previously established method (Kim et al., 2019). TiO_2 samples were digested with a microwave-assisted-acid-digester (Mars 6, CEM corporation, Matthews, NC) and then Ti concentrations were measured using inductively coupled plasma with optical emission spectroscopy (ICP-OES; Optima 8000, PerkinElmer, MA, USA). TiO_2 samples (5 mL) were vigorously shaken and then added to a Teflon microwave digestion vessel (PFA, CEM corporation, Matthews, NC) along with 5 mL of concentrated nitric acid (70%, Trace metal grade, Fisher Scientific, Hampton, NH). TiO_2 samples were heated for 20 min to reach a target temperature of 210 ºC, which was held constant for 45 min. 100 µL of an Se standard (SPEX CertiPrep, NJ, USA) solution with a nominal concentration of 100 mg L^{-1} was added to every 20^{th} sample as a surrogate to monitor the efficiency of the TiO_2 acid-digestion. After the digestion, samples were diluted with HNO_3 (<5% v/v) to a volume of 10

mL and then 1 mL was analyzed using ICP-OES; Optima 8000, PerkinElmer, MA, USA. Yttrium was used as an internal standard and a Ti standard solution was purchased from Inorganic Ventures (VA, USA). The method detection limit (MDL) for Ti samples and ICP-OES was determined using the USEPA procedure (EPA, 2016). This returns the minimum concentration of Ti that can be reliably detected with 99% confidence. For eight replicates, we determined an MDL of 2.1 µg TiO_2 L^{-1}.

2.5 Analysis and Modeling of the Stream Transport Experiments

All stream experiment data were analyzed using concentration-time plot or breakthrough curve (BTC) datasets. A temporal moment analysis of the BTCs was conducted to obtain the mass recovery (M_{rec}), mean arrival time (μ), and variance or measure of the plume spread (σ^2) (Equations 1-3) (Leube et al., 2012). $C(x,t)$ is the concentration at the downstream longitudinal location x and time t.

$$M_{rec} = Q \int C(x,t)dt \quad (1)$$

$$\mu = Q \int tC(x,t)dt \quad (2)$$

$$\sigma^2 = Q \int (t-\mu)^2 C(x,t)dt \quad (3)$$

The stream transport data was modeled using a mobile-immobile model (MIM) that is based on Continuous Time Random Walk (CTRW) theory (Berkowitz et al., 2006; Boano et al., 2007), and built on previous advancements by Roche et al. (Roche et al., 2019b). A key component of this MIM relative to standard ones, is that immobile processes are not assumed to be exponential. The one-dimensional CTRW model conceptualizes mass transport in the stream as a continuous exchange of mass between mobile (water column) and immobile (streambed) domains. Model parameters are relatable to physical and chemical processes in a stream with impermeable

beds (Boano et al., 2007), such as stream velocity and dispersion, temporary storage in low velocity zones, and permanent mass immobilization (e.g., via irreversible filtration). The stream at ND-LEEF has a single low-velocity domain (hyporheic zone) and well-controlled flow conditions (Aubeneau et al., 2014; Roche et al., 2018). Conservative transport is described by a convolution equation of the advection-dispersion equation with a memory kernel (Equation 4).

$$\frac{\partial C(x,t)}{\partial t} = \int_0^t M(t-t') \left[-U \frac{\partial C(x,t')}{\partial x} + D \frac{\partial^2 C(x,t')}{\partial x^2} \right] dt' \quad (4)$$

Where, U (L T^{-1}) is the average mobile zone velocity, D (L^2 T^{-1}) is the longitudinal dispersion coefficient, $C(x,t)$ is the in-stream concentration (M L^{-3}), x is the longitudinal position, t is the elapsed time, and $M(t)$ is the memory kernel determined by the rate of mass immobilization and residence times in the immobile domain, and reaction rates when considering reactive processes. Mass immobilization (i.e., hyporheic exchange) is modeled as a first-order process with rate parameter Λ (T^{-1}), which assumes rapid mixing of mass in the water column, typically a reasonable assumption for a turbulent flow. Residence times in the immobile domain are parameterized with a probability distribution. Previous studies show that a truncated power-law (TPL) distribution is a suitable choice for ND-LEEF streams (Aubeneau et al., 2016, 2014; Dentz et al., 2004). The TPL assumes that residence time probability follows a $\sim t^{-\beta}$ power law up to a truncation timescale (T), after which the probability tempers exponentially. The power law exponent or log-slope (β) of this function represents the slope of the tail of the BTC and describes the residence time in the immobile region. T describes the time point that all reversible mass is recovered.

These hydrodynamic transport parameters were determined using data from RWT BTCs. We found best-fit model parameters by using the objective function developed by Kelly et al. (Kelly et al., 2017), which minimizes summed squared errors (SSE) between modeled and measured concentrations. RWT is a conservative tracer sensitive only to the velocity distribution

in the water column and porous streambeds (McInnis et al., 2014). This allows parameters that describe the purely hydrodynamic processes of the stream (i.e., U, D, Λ, β, and T) to be estimated, which can then be used to predict the specific reactive transport parameters of the TiO_2 NPs. We used the parameters obtained from the 50-m sampling point of the RWT experiments under minimal and thriving biofilm conditions. The transport difference between RWT and the TiO_2 NPs was assumed to be controlled only by parameters that describe permanent mass immobilization in either the mobile or immobile domains, K_{mobile} and $K_{immobile}$, respectively (Roche et al., 2019a). Mathematically, K_{mobile} and $K_{immobile}$, modify Equation 4 as permanent first order removal processes in the mobile and immobile parts of memory function $M(t)$ (Aubeneau et al., 2015a). K_{mobile} (T^{-1}) describes the first-order removal rate of NPs in the mobile domain that includes the water column. $K_{immobile}$ (T^{-1}) describes the first-order removal rate of NPs in the immobile domain that includes the streambed. The use of independent trapping rates allows us to relate changes in best-fit model parameters to physical changes in each domain between experiments. Interactions that occur at the interface between the mobile and immobile phases may be described by either parameter, but there was insufficient data available to distinguish which controls the interfacial processes. As such, the TiO_2 transport parameters were fixed to the best-fit values from RWT experiments (i.e., U, D, Λ, β, T), and then K_{mobile} and $K_{immobile}$ were allowed to vary to obtain a minimized SSE. This modeling approach using CTRW may have limitations such as variabilities in modeling outcomes (e.g., model parameters) depending on the quality (accuracy and precision) of the experimental data, which is attributed to the detection limit of analytical instruments and limited monitoring time (i.e., no long-term observation of irreversibility).

Each of the hydrodynamic and reactive transport parameters will affect the shape of the BTC (Figure 3), as simulated previously (Aubeneau et al., 2015a). In the mobile domain (i.e.,

water column), U will alter the arrival times (e.g., peak, mean) of the BTC, and D will affect the spread of peak. Λ and β will represent the immobile domain effects (i.e., subsurface), which manifests in the tail portion of the BTC. Λ affects the onset concentration of the tail, but it does not affect the slope. A lower Λ means that less mass is entering the subsurface and thus stays in the mobile region longer. This would result in a lower onset concentration of the tail, and subsequently, a lower T since the mass will leave the immobile domain earlier. The inverse of Λ is the average amount of time a particle will spend in the surface before being exchanged with the subsurface. Lower β values will result in longer residence times in the immobile domain and produces heavier tails of the BTC. K_{mobile} represents irreversible uptake in the water column. K_{mobile} will affect the peak concentration and the peak and mean arrival times. It will also affect the onset concentration of the tail and its cutoff but not the onset time, onset concentration, or the slope of the tail. Increasing K_{mobile} will result in a decreased BTC peak concentration and early arrival times as less mass interacts with slower subsurface flows, and the onset concentration and cutoff of the tail will be earlier than for a conservative tracer. As a general qualitative representation, $K_{immobile}$ is the irreversible uptake in the subsurface. $K_{immobile}$ will not affect the peak concentration of its arrival time, but it can affect the shape and length of the tail, which will result in changes to the mean arrival time and T. Increasing $K_{immobile}$ will result in steeper tail slopes with an early T and early mean arrival time.

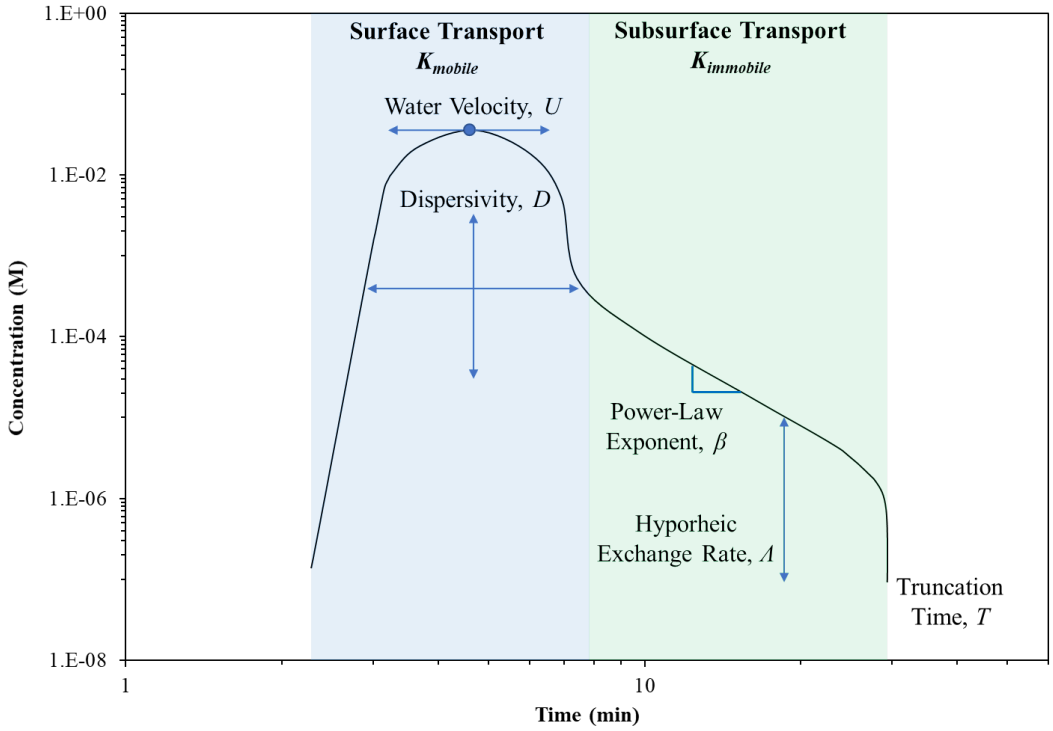

Figure 3. Qualitative example of a theoretical BTC for a nonconservative tracer. Key hydrodynamic parameters (U, D, Λ, β, T) and their effect on the shape of the BTC are shown. Regions of the BTC that are affected by the reactive transport parameter, K_{mobile} and $K_{immobile}$, are shaded in blue and green, respectively.

3.0 RESULTS AND DISCUSSION

3.1 Characterization of the Stream Water and TiO_2 Homoaggregation Behavior

The pH, conductivity, Chl a, and AFDM of the stream were analyzed prior to each experiment (Table 1). TSS and TDS were measured once in June and in September. There were only minimal differences in temperature, pH, conductivity, and TDS. Marked changes in TSS, Chl a, and AFDM from June to September were observed due to seasonal biofilm growth (i.e., Figure 2). Though specific distinctions were not made about the particulate components contributing to the TSS,

because the stream conditions are constant from June to September, the change in TSS was presumably due to the addition of particulate organic matter from in-stream biofilm growth. The background concentration of Ti was below the ICP-OES MDL for all samples.

Table 1. Results of the background parameter measurements for the stream water. TSS and TDS analyses were for a single composite sample developed from six samples taken every 10 m in the stream. All other characteristics reported are for the average and standard deviation of discrete measurements taken every 10 m.

	Month	Value
Temperature	June	24.70 ± 0.66
	Sept.	24.58 ± 2.65
pH	June	8.61 ± 0.03
	Sept.	8.68 ± 0.03
Conductivity (µs)	June	238.12 ± 3.09
	Sept.	252.33 ± 6.51
TSS (mg/L)	June	0.25
	Sept.	4.06
TDS (mg/L)	June	287
	Sept.	396
Chl a (µg/L)	June	0.62 ± 0.10
	Sept.	5.35 ± 0.53
AFDM (mg/cm^2)	June	0.06 ± 0.03
	Sept.	0.63 ± 0.05

The homoaggregation behavior of the TiO_2 NPs in the stream water was assessed by analyzing the changes in hydrodynamic diameter and zeta potential over approximately 1 hr (Figure 4A). In ultrapure water, the initial (<1 min) hydrodynamic diameter of TiO_2 was approximately 261 ± 5.5 nm, and this was constant for 24 hrs (256 ± 2.9 nm, not shown). In contrast, the initial (<1 min) hydrodynamic diameter of TiO_2 in stream water was 648 ± 45 nm, which was significantly larger than the hydrodynamic diameter in ultrapure water ($P < 0.05$). Throughout the experiment, hydrodynamic diameter of TiO_2 increased and reached 865 ± 17 nm

after approximately 1 hr. This marked increase compared to ultrapure water is attributed to the higher conductivity (i.e., ionic strength) of the stream water. In either case though, the addition of TiO_2 to water resulted in the aggregation of particles with a cluster size an order of magnitude greater than the average primary particle size (~15 nm). No significant differences ($P > 0.05$) were observed between filtered and unfiltered stream water (not shown), suggesting that any suspended organic or inorganic matter present in the stream did not affect the stability of the TiO_2 NPs. Similarly, no difference was observed between TiO_2 samples in ultrapure water analyzed after seconds of mixing compared to multiple hours of mixing (not shown). For TiO_2-DOM in stream water, the initial (<1 min) hydrodynamic size was 306 ± 15 nm, and this increased only slightly to 362 ± 31 nm after approximately 1 hr. The significant difference between the hydrodynamic diameters of TiO_2 and TiO_2-DOM in the stream water ($P < 0.05$) suggests that the DOM protects the TiO_2 NPs from aggregation in high ionic strength waters. The average zeta potentials of -18.8 ± 0.53 and -16.1 ± 1.8 mV (pH 8.1) for TiO_2 and TiO_2-DOM in stream water, respectively, were relatively steady over approximately 1 hr (Figure 4B). DOM can adsorb to the NP surface and stabilize them against aggregation (Aiken et al., 2011; Jayalath et al., 2018; Stankus et al., 2011). Though the zeta potential difference between TiO_2 and TiO_2-DOM was significant ($P < 0.05$), the small difference suggests that the enhanced stability caused by DOM was due to steric hindrance rather than electrostatic repulsion from negatively charged functional groups.

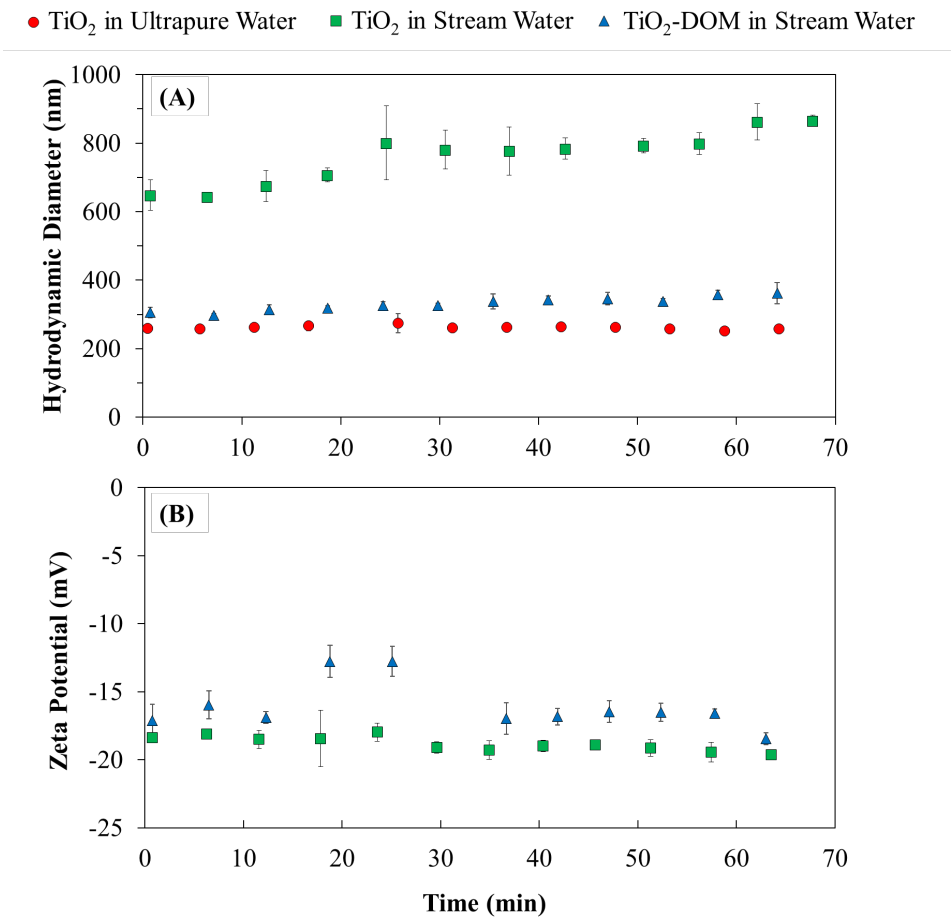

Figure 4. (A) Hydrodynamic size and (A) zeta potential of TiO_2 and TiO_2-DOM in various water samples. The error bars represent one standard deviation of analytical triplicates.

3.2 Temporal Moment Analysis of BTCs

Figure 5a shows the BTCs of TiO_2 and TiO_2-DOM in the presence of minimal biofilms at the 25-m and 50-m sampling points. Log-scale plots are also presented to visually resolve the tail portion of the BTCs (Figure 5b). Figure S2 shows the equivalent BTCs for the conservative tracer, RWT. The results of the temporal moment analyses of the BTCs are provided in Table 2. Under minimal and thriving biofilm conditions, the mass recovery of RWT at 25 m was approximately 94% and 100%, respectively. The recovery decreased to 87% as RWT moved downstream to the 50 m point.

This mass loss of the conservative tracer was presumably due to analytical detection limits and minor non-conservative effects (e.g., volume loss from stream, sorption). Furthermore, we only sampled the water column portion of the stream, and while we assume the subsurface is immobile, there will be some slow advection that manifests as apparent mass loss (Roche et al., 2019a).

For all conditions tested, the mass recovery of TiO_2-DOM was higher than TiO_2. Under minimal biofilm conditions, the mass recovery of TiO_2 at 25 m was only 14% and nearly all the TiO_2 had been retained in the stream by 50 m. Biofilm growth in the stream during these experiments was negligible, so the TiO_2 mass loss was attributed to its interaction with the porous streambed substrate. The D_{50} size ratio (NP:Smallest Media) for TiO_2 and TiO_2-DOM is 0.0015 and 0.00057, respectively, which is much less than the requirement for mechanical filtration to occur in polydisperse granular media (Kerimov et al., 2018). Thus, the major driving force for TiO_2 loss in the streambed was presumably attachment via electrostatic interactions. While the time-scale and detection limits of this study did not allow us to observe the resuspension of the NPs, previous results suggest that particles attached to biogeological media can be remobilized during high-flow events that disturb the streambed (Cushing et al., 1993; Drummond et al., 2014b; Newbold et al., 2005).

Under minimal biofilm conditions, co-releasing DOM with TiO_2 (i.e., TiO_2-DOM) enhanced the transport of TiO_2 compared to experiments using only TiO_2 with mass recoveries at the 25-m and 50-m sampling points of 47% and 32%, respectively. The improved transport is presumably due to the adsorption of DOM onto TiO_2, providing a repulsive or steric coating that minimizes the interaction with the stream substrates. Because DOM and TiO_2 were simultaneously released to the stream without any pre-mixing, this suggests the adsorption process is fast relative to the stream velocity. This hypothesis is supported by previous lab-scale results describing the

447 rapid adsorption of DOM onto TiO_2 (Jayalath et al., 2018; Kim and Doudrick, 2019). The mean
448 (t_m) and peak (t_p) arrival times of TiO_2 and TiO_2-DOM were approximately the same (e.g., t_m = 8.5
449 min at 50 m), but there was considerably more mass recovered with TiO_2-DOM with a percent
450 change of 87%. The delivery of NPs to the streambed is controlled by advective hyporheic
451 exchange and gravitational settling would be negligible because both TiO_2 and TiO_2-DOM
452 particles/aggregates are <1,000 μm (Figure 4). Collectively, these outcomes suggest that the
453 presence of DOM reduces the interaction of TiO_2 with streambed substrates, but it does not alter
454 the flow pathway of TiO_2 (e.g., more transporting in the water column).

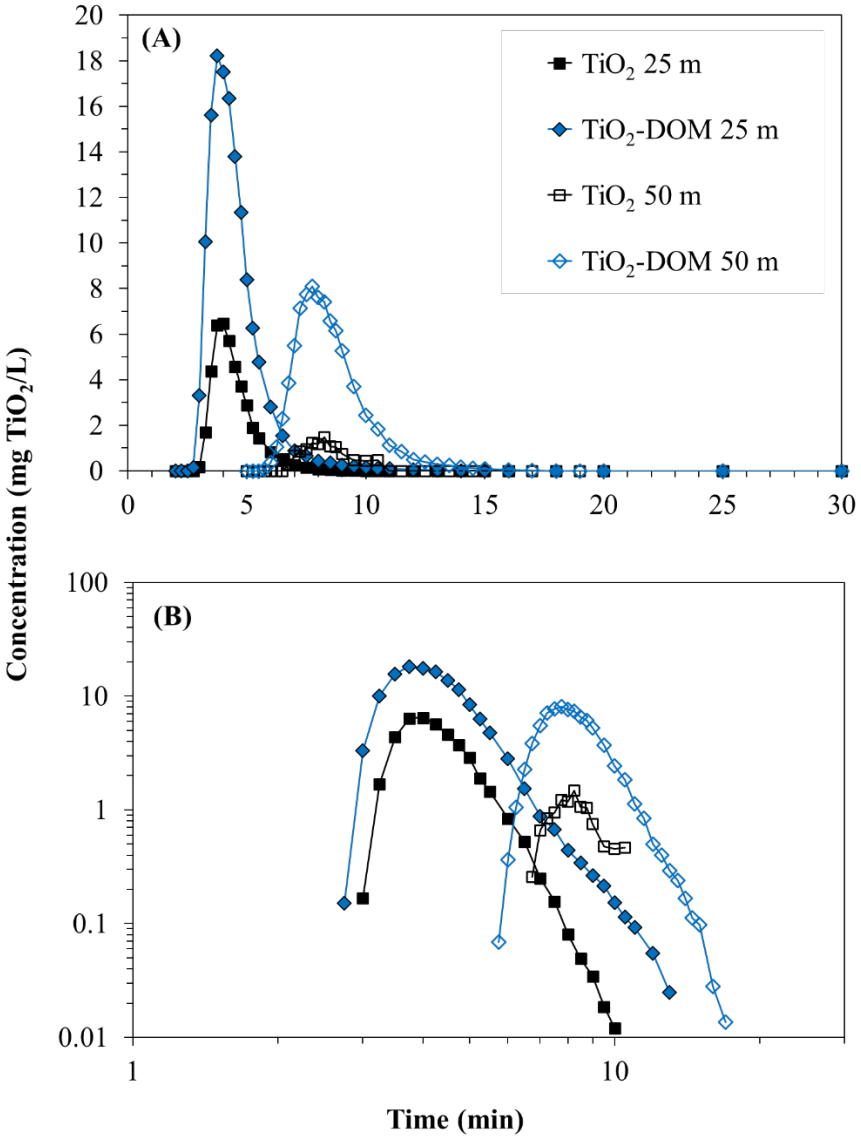

455

456 **Figure 5**. BTCs of TiO_2 for samples taken at 25 m and 50 m in a stream with minimal biofilm

457 growth. (A) Concentration-time plot and (B) log concentration-log time plot.

458

459

460 **Table 2**. Temporal moment analysis of BTCs of RWT and P90 in June and Sept.

Sample	Biofilm Condition	Sampling Distance (m)	Mass Recovery (%)	Mean Arrival Time, t_m (min)	Peak Arrival Time, t_p (min)	Variance (min^2)
RWT	Minimal	25	94	6.40	4.50	43
		50	87	11.3	8.52	57
	Thriving	25	100	11.4	6.50	124
		50	87	22.9	15.5	269
TiO_2	Minimal	25	14	4.40	4.00	0.7
		50	4.2	8.50	8.25	1.0
	Thriving	25	2.2	7.00	6.00	2.5
		50	0.50	15.2	13.7	0.7
TiO_2-DOM	Minimal	25	47	4.50	3.75	1.2
		50	32	8.50	7.75	2.2
	Thriving	25	43	9.10	7.25	10
		50	36	19.1	17.0	19

461

462 The transport experiments were repeated in September when biofilms were ubiquitous in
463 the stream (Figure 2C), with filamentous biofilms observed within water column and adhered to
464 the streambed-water interface. The transport of TiO_2 was considerably reduced in the presence of
465 thriving biofilm conditions with mass recoveries less than 3% observed (Figure 6, Table 2).
466 Biofilms in the water column were visually inspected after the transport experiment, and there
467 were noticeable white patches on entrapped TiO_2 (Figure S3). Small samples of biofilms were
468 taken at five points in the stream (0, 5, 10, 25, 50 m) and then analyzed for TiO_2 mass. Assuming
469 the TiO_2 loading in the biofilm samples was homogeneous and representative of all biofilms at
470 each sampling point, most of the TiO_2 mass loss (>95%, Figure S4) occurred in the first 5 m of the
471 stream, with nearly ~85% of the total TiO_2 measured being captured near the TiO_2 sample injection
472 point (i.e., ~0 to 0.5 m). This outcome suggests that the mass loss of TiO_2 due to biofilms is rapid
473 compared to the stream velocity.

The mass recovery for TiO_2-DOM at 25 m and 50 m (43% and 36%) in the presence of thriving biofilms was higher than TiO_2 (2.2% and 0.5%). Furthermore, the mass recovery for TiO_2-DOM under thriving biofilm conditions was not markedly different compared to minimal biofilms conditions (<5% difference). The mean arrival time for TiO_2-DOM (19.1 min at 50 m) was greater than TiO_2 (15.2 m at 50 m) in the presence of thriving biofilms. This observation contrasted with the similar arrival times observed under minimal biofilms conditions. Thus, the presence of biofilms considerably increases the mass loss of TiO_2 NPs, whereas in the presence of DOM the biofilms retard the transport of TiO_2 without irreversibly trapping it.

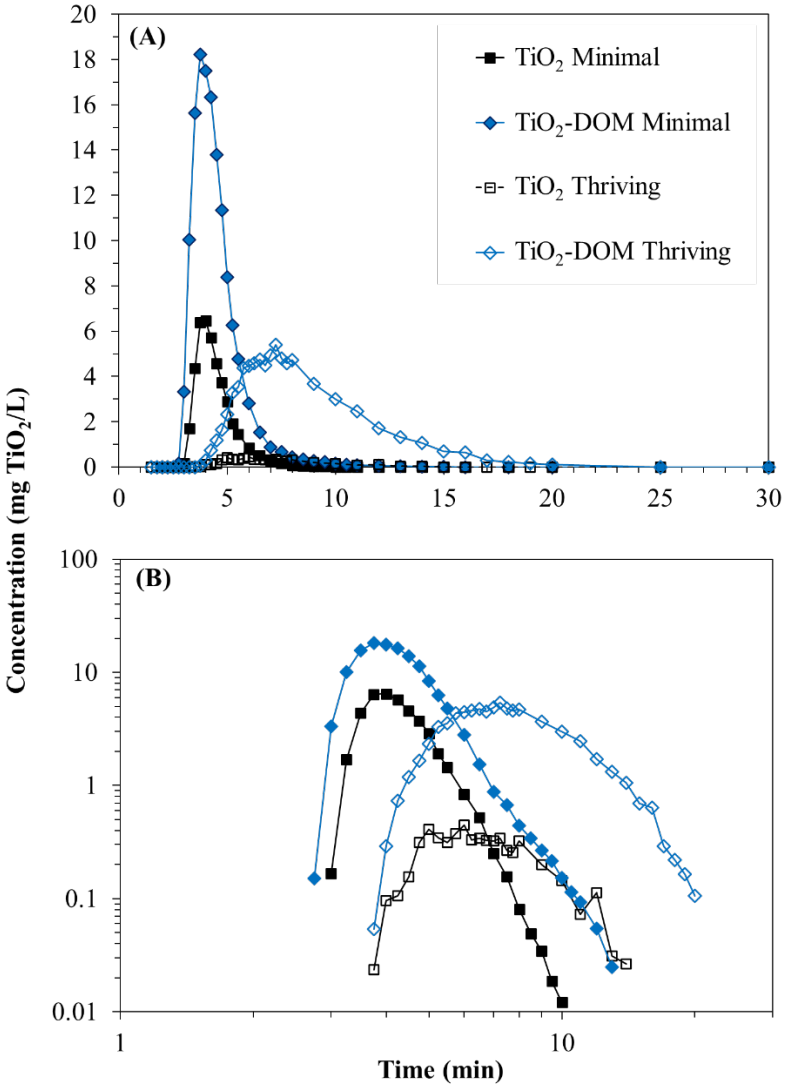

Figure 6. BTCs of TiO_2 and TiO_2-DOM for samples taken at 25 m in a stream with thriving biofilms. (A) Concentration-time plot and (B) log concentration-log time plot.

3.4 Modeling the Transport of TiO_2 NPs in Streams

The best-fit model parameters were obtained from the RWT BTCs for minimal and thriving biofilm conditions (Table 3). The accompanying experimental and modeled BTCs for RWT are shown in Figure 7. The model was suitable for the early, peak, tail, and truncation time portions of the RWT BTCs, which highlights its ability to capture a range of spatio-temporal phases. The

presence of thriving biofilms altered the hydrodynamic transport parameters. The water column velocity (U) decreased approximately 25% and the dispersivity (D) increased approximately 50%, which indicates increased mixing in the stream. The hyporheic exchange rate (A) increased approximately 30%, indicating a higher probability of NPs being carried by the stream water into the streambed. The power-law exponent (β) decreased approximately 10%, indicating that NPs spent an increased time in the streambed before moving back into the water column. This would increase the chances of interaction with the streambed media. The parameter values from the 25-m and 50-m sampling points were in relative agreement (Table S1), but some notable differences were observed (e.g., U for thriving). One of the key assumptions of the model is that the stream is well mixed and hydraulically identical throughout the reach, but the observed differences suggest some heterogeneity exists. Overall, the transport parameters were quantitatively similar to previous conservative tracer studies conducted in the same stream at ND-LEEF (Roche et al., 2019a, Aubeneau et al., 2016).

507 **Table 3**. Best-fit model parameters for the conservative tracer (RWT) BTCs under minimal and
508 thriving biofilm. Values are averaged for 25-m and 50-m sampling points and assumes the flow
509 behavior is consistent throughout the stream. The parameters are water column velocity (U),
510 generalized dispersion coefficient (D), hyporheic exchange rate (Λ), power-law exponent of the
511 BTC tail (β), and power-law truncation time (T).

Parameter	Minimal Biofilms	Thriving Biofilms
U ($\times 10^{-2}$ m/s)	12.3	9.50
D ($\times 10^{-2}$ m^2/s)	2.35	4.95
Λ ($\times 10^{-2}$ s^{-1})	8.97	13.0
β	0.959	0.869
T (min)	128	114

512

513

514

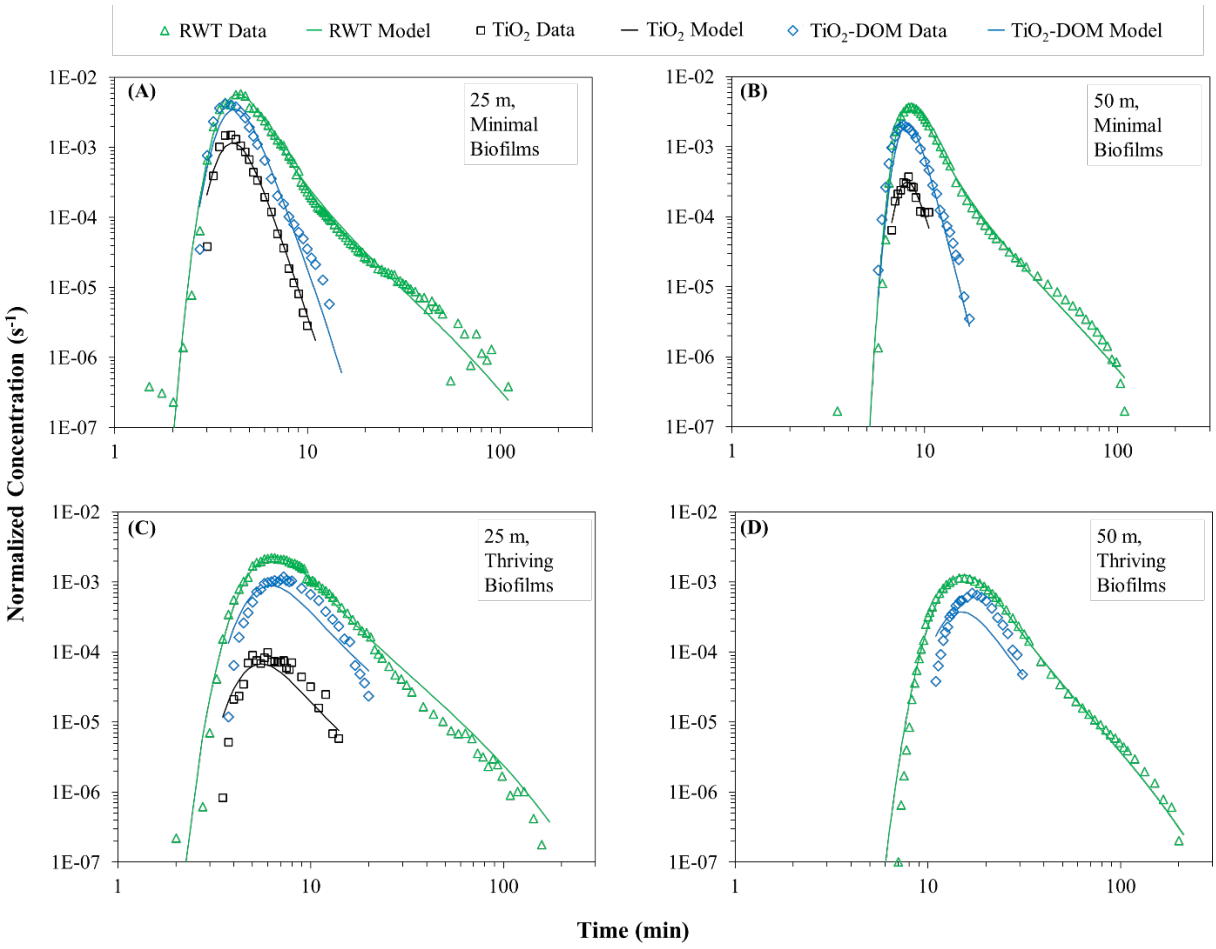

Figure 7. Computational modeling fits for RWT, TiO_2, and TiO_2-DOM under minimal (A, B) and thriving (C, D) biofilm conditions at 25 m (A, C) and 50 m (B, D) sampling points.

Figure 7 shows the experimental and modeled BTCs for TiO_2 and TiO_2-DOM under minimal and thriving biofilm conditions at the 25-m and 50-m sampling points. No model fit was obtained for TiO_2 at 50 m under thriving biofilm conditions because data was only obtained at three data points due to the large mass loss. Under minimal biofilm conditions (Figures 7A and 7B), relatively good model fits were obtained, which attests to the model's ability to capture a broad range of transport processes (e.g., aggregation, physical retention, chemical sorption). Under

thriving biofilm conditions (Figures 7C and 7D), the predictive capability of the model was reduced.

There are two explanations for the diminished capability of the model under thriving biofilm conditions. The first reason is related to the attachment behavior of the NPs to biofilms. The model assumes the mass removal process is irreversible, at a first-order rate described by the K parameters. If the interaction between the biofilms and the NPs is a reversible, attachment-detachment process, then this would be reflected in an equally de-scaled U and D (i.e., U and D are less than what is predicted by the RWT data) that is a surrogate for a retardation factor. The model predicted earlier arrival times than the experimental data, which is influenced by U and D. Thus, de-scaling U and D equally would increase the predicted arrival time and more closely matching the experimental data. This speculation is supported by the moment analysis outcomes (Figure 3). The mean arrival times for TiO_2 and TiO_2-DOM were similar under minimal biofilm conditions, but different under thriving conditions, which suggests differing retardation factors could be playing a role for the differing surface chemistries of the two TiO_2 NPs. The second reason is related to the model determination of the K values. During model optimization of the K values, the SSE continued to decrease until a maximum or minimum K value was reached (i.e., 10^{-8}); however, there was a limiting point where decreasing the K by an order of magnitude minimized the SSE but did not improve the model fit (e.g., Figure S5 for $K_{mobile)}$. Inaccurate K values would incorrectly predict the mass removed, resulting in BTCs that are shifted below or above the experimental data (e.g., Figure 7D).

To account for the issues with the model for thriving biofilm conditions, U and D were scaled equally and then K_{mobile} and $K_{immobile}$ parameters were adjusted to obtain a better fit by manually minimizing the SSE. The Λ, β, T parameters were not adjusted. For example, for TiO_2-

548 DOM at 50 m under thriving biofilm conditions, the shape of the modeled BTC (Figure 7D) was
549 too wide with a shallow tail slope and predicted concentrations that were too low and early. This
550 means the model was overestimating U and D, and both K_{mobile} and $K_{immobile}$ predictions had
551 convergence errors. To account for this, U and D were first de-scaled equally to account for
552 reversible attachment processes, and then the K parameters were optimized. K_{mobile} decreased and
553 $K_{immobile}$ increased, thus reducing the mass loss in the water column but increasing the mass loss in
554 the streambed, respectively.

555 The parameter results for minimal and thriving biofilm conditions are shown in Table 4,
556 and the adjusted BTCs are shown in Figure 8. Also listed in Table 4 is the $K_{mobile}/K_{immobile}$ ratio,
557 which provides some insight into where the mass loss of TiO_2 occurred in the stream. The K ratio
558 for minimal and thriving biofilm conditions was greater for TiO_2 compared to TiO_2-DOM,
559 suggesting greater mass loss in the mobile domain. This model outcome agreed with the larger
560 mass loss observed for TiO_2 (Table 2). For TiO_2, the presence of thriving biofilm conditions
561 resulted in a higher K ratio compared to minimal biofilm conditions. The increased K_{mobile} was
562 presumably due to mass loss to biofilms present in the water column (Figure 2C). For TiO_2-DOM,
563 the K ratio was similar for both biofilm conditions, which agrees with experimental results (Table
564 2) that indicated the influence of biofilms on the mass recovery of TiO_2-DOM was minimal. The
565 modeled parameters reiterate the ability of DOM to reduce interactions of TiO_2 with biofilms and
566 the streambed substrate.

567 As a demonstration of the usefulness of the model and implications of the findings, the
568 distance the TiO_2 NPs must travel in the stream to reach a desired percent mass retention was
569 determined (Table 4, Figure 9). For example, 99.9% of TiO_2 NPs would be removed from the
570 water column and retained in the streambed after traveling approximately 90 m and 50 m for

571 minimal and thriving biofilm conditions, respectively, and the presence of DOM more than
572 doubles the distance the NPs will travel.

573

574 **Table 4**. K_{mobile} and $K_{immobile}$ best-fit model parameters for TiO_2 and TiO_2-DOM under minimal
575 and thriving biofilm conditions and 25-m and 50-m sampling points.

	Minimal Biofilms		Thriving Biofilms	
Parameter	**TiO_2**	**TiO_2-DOM**	**TiO_2**	**TiO_2-DOM**
K_{mobile} ($\times 10^{-4}$ s^{-1})	50	0.5	100	0.04
$K_{immobile}$ ($\times 10^{-4}$ s^{-1})	60	73	20	13
K_{mobile} / $K_{immobile}$	0.8	0.007	5	0.003
U ($\times 10^{-2}$ m/s)	12.3		8.66	7.56
D ($\times 10^{-2}$ m^2/s)	2.35		3.51	4.49
Distance to Retain 99.9% Mass (m)	120	310	60	410

576

577

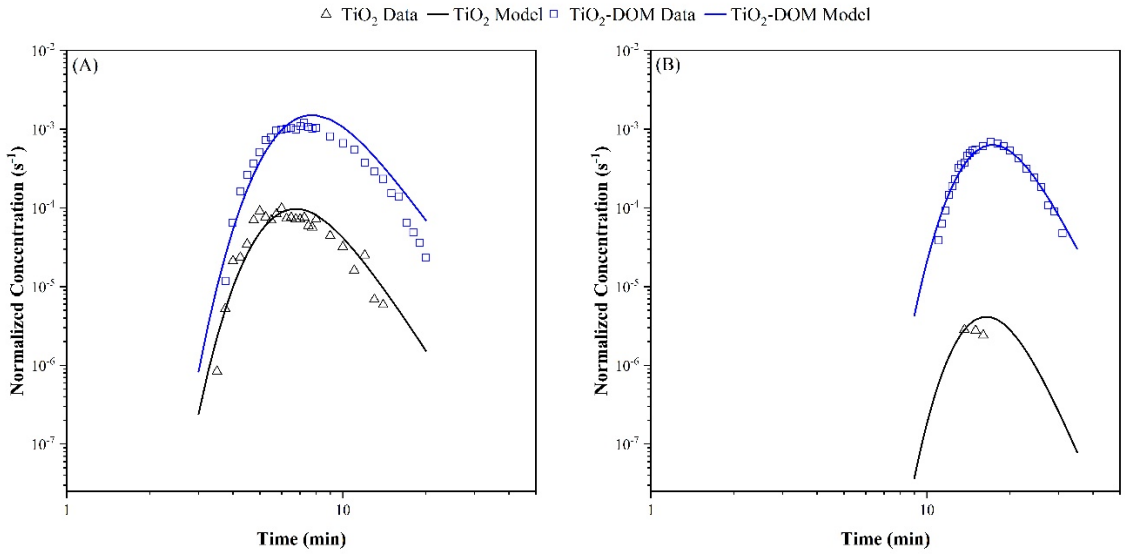

578

579 **Figure 8**. Manually adjusted model fits for the TiO_2 and TiO_2-DOM BTCs under thriving biofilm
580 conditions at sampling distances of (A) 25 m (A) and (B) 50 m.

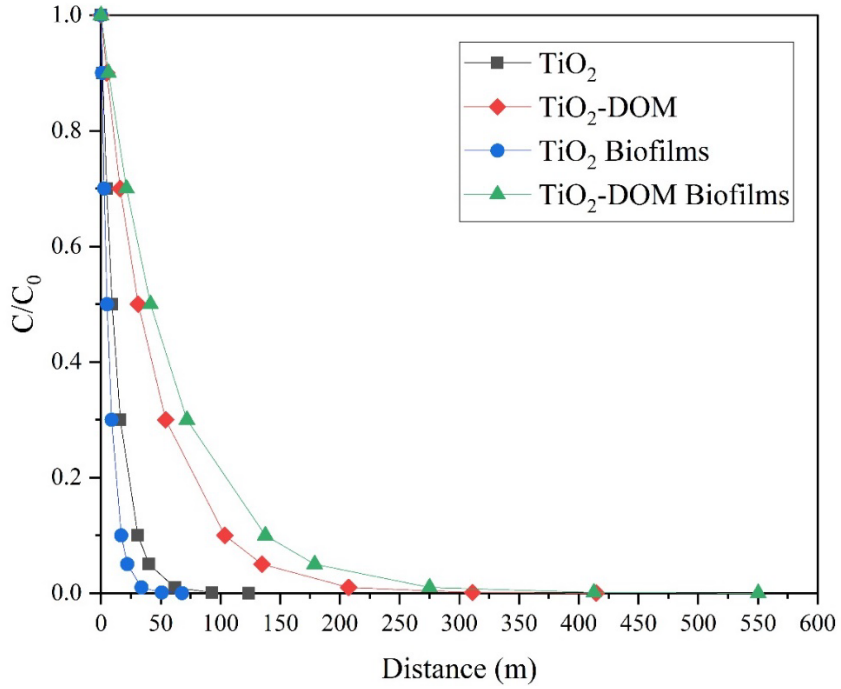

Figure 9. Predicted normalized concentrations of TiO_2 and TiO_2-DOM under minimal and thriving biofilm conditions as a function of distance traveled in the stream.

4.0 CONCLUSION

The transport of NPs in streams is heavily influenced by the presence of biofilms and DOM. When biofilms are present in streams they can immobilize NPs, resulting in diminished downstream transport. This may be exacerbated by the homoaggregation of NPs in streams, especially those with high ionic strength. The presence of DOM stabilizes NPs against homoaggregation and mitigates the impact of biofilms, thus enhancing transport. Whereas TiO_2 NPs are presumably immobilized in the biofilms, the presence of DOM causes biofilm-NP interactions to be reversible. These conclusions should be confirmed by extensive lab-scale studies. When DOM interacts with TiO_2 NPs, it adsorbs to and covers the surface of the NP, thus changes the surface "identity" of the

595 NP (Kim and Doudrick, 2019; Louie et al., 2016, 2013). So, though the results presented herein
596 are specific for TiO_2, the transport of other NPs will presumably be similar when DOM
597 concentrations are high enough that they coat the surface of the NP. Collectively these findings
598 have significant implications for real world transport of TiO_2. For example, TiO_2 NPs that are
599 present in wastewater effluent will likely be covered with organic macromolecules that stabilize
600 them from aggregation and reduce interactions with biogeological media present in the stream.
601

Acknowledgments

This material is based upon work supported by the National Science Foundation under grant no. CBET-1705770. We especially want to thank ND-LEEF for use of the experimental streams. The authors thank the Center for Environmental Science & Technology at Notre Dame for access to instrumentation, including the IC, TOC, ICP-OES, and microwave digester.

Appendix. Supplementary Materials

Download Acrobat PDF File.

References

Aiken, G.R., Hsu-kim, H., Ryan, J.N., 2011. Influence of Dissolved Organic Matter on the Environmental Fate of Metals, Nanoparticles, and Colloids. Environ. Sci. Technol. 45, 3196–3201. https://doi.org/10.1021/es103992s

Allen, N.S., Edge, M., Ortega, A., Liauw, C.M., Stratton, J., McIntyre, R.B., 2002. Behaviour of nanoparticle (ultrafine) titanium dioxide pigments and stabilisers on the photooxidative stability of water based acrylic and isocyanate based acrylic coatings. Polym. Degrad. Stab. 78, 467–478. https://doi.org/10.1016/S0141-3910(02)00189-1

Areepitak, T., Ren, J.H., 2011. Model Simulations of Particle Aggregation Effect on Colloid Exchange between Streams and Streambeds. Environ. Sci. Technol. 45, 5614–5621. https://doi.org/10.1021/es200586v

Arnon, S., Marx, L.P., Searcy, K.E., Packman, A.I., 2010. Effects of overlying velocity, particle size, and biofilm growth on stream--subsurface exchange of particles. Hydrol. Process. 24, 108–114.

Aubeneau, A.F., Drummond, J.D., Schumer, R., Bolster, D., Tank, J.L., Packman, A.I., 2015a. Effects of benthic and hyporheic reactive transport on breakthrough curves. Freshw. Sci. 34, 301–315.

Aubeneau, A.F., Hanrahan, B., Bolster, D., Tank, J., 2016. Biofilm growth in gravel bed streams controls solute residence time distributions. J. Geophys. Res. Biogeosciences 121, 1840–1850.

Aubeneau, A.F., Hanrahan, B., Bolster, D., Tank, J.L., 2014. Substrate size and heterogeneity control anomalous transport in small streams. Geophys. Res. Lett. 41, 8335–8341.

Aubeneau, A.F., Martin, R.L., Bolster, D., Schumer, R., Jerolmack, D., Packman, A., 2015b.

Fractal patterns in riverbed morphology produce fractal scaling of water storage times. Geophys. Res. Lett. 42, 5309–5315.

Battin, T.J., Kammer, F.V.D., Weilhartner, A., Ottofuelling, S., Hofmann, T., 2009. Nanostructured TiO2: Transport Behavior and Effects on Aquatic Microbial Communities under Environmental Conditions. Environ. Sci. Technol. 43, 8098–8104. https://doi.org/10.1021/es9017046

Battin, T.J., Kaplan, L.A., Findlay, S., Hopkinson, C.S., Marti, E., Packman, A.I., Newbold, J.D., Sabater, F., 2008. Biophysical controls on organic carbon fluxes in fluvial networks. Nat. Geosci. 2008 12 1, 95–100. https://doi.org/10.1038/ngeo101

Battin, T.J., Kaplan, L.A., Newbold, J.D., Hansen, C.M.E., 2003. Contributions of microbial biofilms to ecosystem processes in stream mesocosms. Nature 426, 439–442.

Berkman, J.A.H., Canova, M.G., 2007. Chapter A7. Section 7.4. Algal biomass indicators, Techniques of Water-Resources Investigations. Reston, VA. https://doi.org/10.3133/twri09A7.4

Berkowitz, B., Cortis, A., Dentz, M., Scher, H., 2006. Modeling non-Fickian transport in geological formations as a continuous time random walk. Rev. Geophys. 44.

Boano, F., Packman, A.I., Cortis, A., Revelli, R., Ridolfi, L., 2007. A continuous time random walk approach to the stream transport of solutes. Water Resour. Res. 43. https://doi.org/10.1029/2007WR006062

Bolster, D., Roche, K.R., Morales, V.L., 2019. Recent advances in anomalous transport models for predicting contaminants in natural groundwater systems. Curr. Opin. Chem. Eng. https://doi.org/10.1016/j.coche.2019.09.006

Boncagni, N.T., Otaegui, J.M., Warner, E., Curran, T., Ren, J.H., De Cortalezzi, M.M.F., 2009.

Exchange of TiO2 Nanoparticles between Streams and Streambeds. Environ. Sci. Technol. 43, 7699–7705. https://doi.org/10.1021/es900424n

Choi, S., Johnston, M. V., Wang, G.S., Huang, C.P., 2017. Looking for engineered nanoparticles (ENPs) in wastewater treatment systems: Qualification and quantification aspects. Sci. Total Environ. 590–591, 809–817. https://doi.org/10.1016/j.scitotenv.2017.03.061

Cushing, C.E., Minshall, G.W., Newbold, J.D., 1993. Transport dynamics of fine particulate organic matter in two Idaho streams. Limnol. Oceanogr. 38, 1101–1115.

Darlington, T.K., Neigh, A.M., Spencer, M.T., Nguyen, O.T., Oldenburg, S.J., Guyen, O.T.N., Oldenburg, S.J., Nguyen, O.T., Oldenburg, S.J., Guyen, O.T.N., Oldenburg, S.J., 2009. NANOPARTICLE CHARACTERISTICS AFFECTING ENVIRONMENTAL FATE AND TRANSPORT THROUGH SOIL. Environ. Toxicol. Chem. 28, 1191–1199. https://doi.org/10.1897/08-341.1

Dentz, M., Cortis, A., Scher, H., Berkowitz, B., 2004. Time behavior of solute transport in heterogeneous media: Transition from anomalous to normal transport. Adv. Water Resour. 27, 155–173. https://doi.org/10.1016/j.advwatres.2003.11.002

Domingos, R.F., Tufenkji, N., Wilkinson, K.J., 2009. Aggregation of Titanium Dioxide Nanoparticles: Role of a Fulvic Acid. Environ. Sci. Technol. 43, 1282–1286. https://doi.org/10.1021/es8023594

Drummond, J.D., Aubeneau, A.F., Packman, A.I., 2014a. Stochastic modeling of fine particulate organic carbon dynamics in rivers. Water Resour. Res. 50, 4341–4356. https://doi.org/10.1002/2013WR014665

Drummond, J.D., Davies-Colley, R.J., Stott, R., Sukias, J.P., Nagels, J.W., Sharp, A., Packman, A.I., 2014b. Retention and remobilization dynamics of fine particles and microorganisms in

680 pastoral streams. Water Res. 66, 459–472. https://doi.org/10.1016/J.WATRES.2014.08.025
681 El-Sherbiny, S., Morsy, F., Samir, M., Fouad, O.A., 2014. Synthesis, characterization and
682 application of TiO2 nanopowders as special paper coating pigment. Appl. Nanosci. 4, 305–
683 313. https://doi.org/10.1007/s13204-013-0196-y
684 EPA, 2016. Office of Water Definition and Procedure for the Determination of the Method
685 Detection Limit, Revision 2.
686 EPA, 1991. ESS Method 150.1: Chlorophyll - Spectrophotometric. Madison.
687 Fei Yin, Z., Wu, L., Gui Yang, H., Hua Su, Y., Yin, Z.F.Z.F., Wu, L., Yang, H.G., Su, Y.H., Fei
688 Yin, Z., Wu, L., Gui Yang, H., Hua Su, Y., Yin, Z.F.Z.F., Wu, L., Yang, H.G., Su, Y.H.,
689 2013. Recent progress in biomedical applications of titanium dioxide. Phys. Chem. Chem.
690 Phys. 15, 4844–4858. https://doi.org/10.1039/c3cp43938k
691 Gondikas, A.P., Von Der Kammer, F., Reed, R.B., Wagner, S., Ranville, J.F., Hofmann, T.,
692 2014. Release of TiO2 nanoparticles from sunscreens into surface waters: A one-year
693 survey at the old danube recreational lake. Environ. Sci. Technol. 48, 5415–5422.
694 https://doi.org/10.1021/es405596y
695 Isaacson, C.W.C., Bouchard, D.D.C., 2010. Effects of Humic Acid and Sunlight on the
696 Generation and Aggregation State of Aqu/C60 Nanoparticles. Environ. Sci. Technol. 44,
697 8971–8976. https://doi.org/10.1021/es103029k
698 Jayalath, S., Wu, H., Larsen, S.C., Grassian, V.H., 2018. Surface Adsorption of Suwannee River
699 Humic Acid on TiO2 Nanoparticles: A Study of pH and Particle Size. Langmuir.
700 https://doi.org/10.1021/acs.langmuir.8b00300
701 Johnson, A.C., Bowes, M.J., Crossley, A., Jarvie, H.P., Jurkschat, K., Jürgens, M.D., Lawlor,
702 A.J., Park, B., Rowland, P., Spurgeon, D., Svendsen, C., Thompson, I.P., Barnes, R.J.,

Williams, R.J., Xu, N., 2011. An assessment of the fate, behaviour and environmental risk associated with sunscreen TiO2 nanoparticles in UK field scenarios. Sci. Total Environ. 409, 2503–2510. https://doi.org/10.1016/j.scitotenv.2011.03.040

Keller, A.A., Vosti, W., Wang, H., Lazareva, A., 2014. Release of engineered nanomaterials from personal care products throughout their life cycle. J. Nanoparticle Res. 16, 2489. https://doi.org/10.1007/s11051-014-2489-9

Kelly, J.F., Bolster, D., Meerschaert, M.M., Drummond, J.D., Packman, A.I., 2017. FracFit: A robust parameter estimation tool for fractional calculus models. Water Resour. Res. 53, 2559–2567. https://doi.org/10.1002/2016WR019748

Kerimov, A., Mavko, G., Mukerji, T., Al Ibrahim, M.A., 2018. Mechanical trapping of particles in granular media. Phys. Rev. E 97, 22907. https://doi.org/10.1103/PhysRevE.97.022907

Kim, J., Doudrick, K., 2019. Emerging investigator series: protein adsorption and transformation on catalytic and food-grade TiO2 nanoparticles in the presence of dissolved organic carbon. Environ. Sci. 6, 1688–1703. https://doi.org/10.1039/c9en00130a

Kim, J., Roche, K.R., Sticha, J., Shogren, A.J., Bolster, D., Doudrick, K., 2019. Transport of food- and catalytic-grade titanium dioxide nanoparticles in controlled field streams with varying streambed and biofilm conditions. Environ. Sci. Nano 6, 3454–3466. https://doi.org/10.1039/c9en01007f

Leube, P.C., Nowak, W., Schneider, G., 2012. Temporal moments revisited: Why there is no better way for physically based model reduction in time. Water Resour. Res. 48, 11527. https://doi.org/10.1029/2012WR011973

Li, K., Chen, Y., 2012. Effect of natural organic matter on the aggregation kinetics of CeO2 nanoparticles in KCl and CaCl2 solutions: Measurements and modeling. J. Hazard. Mater.

209–210, 264–270. https://doi.org/10.1016/j.jhazmat.2012.01.013

Louie, S.M., Tilton, R.D., Lowry, G. V, 2016. Critical review: impacts of macromolecular coatings on critical physicochemical processes controlling environmental fate of nanomaterials. Environ. Sci. 3, 283–310. https://doi.org/10.1039/c5en00104h

Louie, S.M., Tilton, R.D., Lowry, G. V, 2013. Effects of Molecular Weight Distribution and Chemical Properties of Natural Organic Matter on Gold Nanoparticle Aggregation. Environ. Sci. Technol. 47, 4245–4254. https://doi.org/10.1021/es400137x

Lowry, G. V., Hill, R.J., Harper, S., Rawle, A.F., Hendren, C.O., Klaessig, F., Nobbmann, U., Sayre, P., Rumble, J., 2016. Guidance to improve the scientific value of zeta-potential measurements in nanoEHS. Environ. Sci. Nano 3, 953–965. https://doi.org/10.1039/C6EN00136J

McInnis, D.P., Bolster, D., Maurice, P.A., 2014. Natural organic matter transport modeling with a continuous time random walk approach. Environ. Eng. Sci. 31, 98–106. https://doi.org/10.1089/ees.2013.0331

Minshall, G.W., Thomas, S.A., Newbold, J.D., Monaghan, M.T., Cushing, C.E., 2000. Physical factors influencing fine organic particle transport and deposition in streams. J. North Am. Benthol. Soc. 19, 1–16. https://doi.org/10.2307/1468278/ASSET/IMAGES/LARGE/I0887-3593-19-1-1-F03.JPEG

Nason, J.A., McDowell, S.A., Callahan, T.W., 2012. Effects of natural organic matter type and concentration on the aggregation of citrate-stabilized gold nanoparticles. J. Environ. Monit. 14, 1885–1892. https://doi.org/10.1039/c2em00005a

Newbold, J.D., Thomas, S.A., Minshall, G.W., Cushing, C.E., Georgian, T., 2005. Deposition, benthic residence, and resuspension of fine organic particles in a mountain stream. Limnol.

Oceanogr. 50, 1571–1580.

Packman, A.I., Brooks, N.H., Morgan, J.J., 2000. Kaolinite exchange between a stream and streambed: Laboratory experiments and validation of a colloid transport model. Water Resour. Res. 36, 2363–2372. https://doi.org/10.1029/2000WR900058

Pan, B., Xing, B.S., 2012. Applications and implications of manufactured nanoparticles in soils: a review. Eur. J. Soil Sci. 63, 437–456. https://doi.org/10.1111/j.1365-2389.2012.01475.x

Potter, B.B., Wimsatt, J.C., 2005. Method 415.3 - Determination of total organic carbon, dissolved organic carbon and specific UV absorbance at 254 nm in source water and drinking water. Washington D.C.

Ren, J.H., Packman, A.I., 2005. Coupled stream-subsurface exchange of colloidal hematite and dissolved zinc, copper, and phosphate. Environ. Sci. Technol. 39, 6387–6394. https://doi.org/10.1021/es050168q

Roche, K.R., Blois, G., Best, J.L., Christensen, K.T., Aubeneau, A.F., Packman, A.I., 2018. Turbulence Links Momentum and Solute Exchange in Coarse-Grained Streambeds. Water Resour. Res. 54, 3225–3242. https://doi.org/10.1029/2017WR021992

Roche, K.R., Drummond, J.D., Boano, F., Packman, A.I., Battin, T.J., Hunter, W.R., 2017. Benthic biofilm controls on fine particle dynamics in streams. Water Resour. Res. 53, 222–236. https://doi.org/10.1002/2016WR019041

Roche, K. R., Li, A., Bolster, D., Wagner, G.J., Packman, A.I., 2019. Effects of Turbulent Hyporheic Mixing on Reach-Scale Transport. Water Resour. Res. 55, 3780–3795. https://doi.org/10.1029/2018WR023421

Roche, K.R., Shogren, A.J., Aubeneau, A., Tank, J.L., Bolster, D., 2019. Modeling Benthic Versus Hyporheic Nutrient Uptake in Unshaded Streams With Varying Substrates. J.

Geophys. Res. Biogeosciences 124, 367–383. https://doi.org/10.1029/2018JG004684

Shi, H., Magaye, R., Castranova, V., Zhao, J., 2013. Titanium dioxide nanoparticles: a review of current toxicological data. Part. Fibre Toxicol. 10, 15. https://doi.org/10.1186/1743-8977-10-15

Shogren, A.J., Tank, J.L., Andruszkiewicz, E., Olds, B., Mahon, A.R., Jerde, C.L., Bolster, D., 2017. Controls on eDNA movement in streams: Transport, Retention, and Resuspension. Sci. Rep. 7, 11. https://doi.org/10.1038/s41598-017-05223-1

Stankus, D.P., Lohse, S.E., Hutchison, J.E., Nason, J.A., 2011. Interactions between Natural Organic Matter and Gold Nanoparticles Stabilized with Different Organic Capping Agents. Environ. Sci. Technol. 45, 3238–3244. https://doi.org/10.1021/es102603p

Thio, B.J.R., Zhou, D., Keller, A.A., 2011. Influence of natural organic matter on the aggregation and deposition of titanium dioxide nanoparticles. J. Hazard. Mater. 189, 556–63. https://doi.org/10.1016/j.jhazmat.2011.02.072

Vindedahl, A.M., Strehlau, J.H., Arnold, W.A., Penn, R.L., 2016. Organic matter and iron oxide nanoparticles: aggregation, interactions, and reactivity. Environ. Sci. 3, 494–505. https://doi.org/10.1039/c5en00215j

Volder, M.F.L. De, Tawfick, S.H., Baughman, R.H., Hart, A.J., De Volder, M.F.L.L., Tawfick, S.H., Baughman, R.H., Hart, A.J., 2013. Carbon nanotubes: present and future commercial applications. Science (80-.). 339, 535–9. https://doi.org/10.1126/science.1222453

Wang, M., Gao, B., Tang, D., 2016. Review of key factors controlling engineered nanoparticle transport in porous media. J. Hazard. Mater. https://doi.org/10.1016/j.jhazmat.2016.06.065

Weishaar, J.L., Aiken, G.R., Bergamaschi, B.A., Fram, M.S., Fujii, R., Mopper, K., 2003. Evaluation of Specific Ultraviolet Absorbance as an Indicator of the Chemical Composition

and Reactivity of Dissolved Organic Carbon. Environ. Sci. Technol. 37, 4702–4708. https://doi.org/10.1021/ES030360X

Westerhoff, P., Song, G.X., Hristovski, K., Kiser, M.A., 2011. Occurrence and removal of titanium at full scale wastewater treatment plants: implications for TiO2 nanomaterials. J. Environ. Monit. 13, 1195–1203. https://doi.org/10.1039/c1em10017c

Zhang, Q., Huang, J.-Q.J.-Q.J.Q., Qian, W.-Z.Z.W.-Z., Zhang, Y.-Y.Y.-Y.Y.Y., Wei, F., 2013. The road for nanomaterials industry: a review of carbon nanotube production, post-treatment, and bulk applications for composites and energy storage. Small 9, 1237–1265. https://doi.org/10.1002/smll.201203252

Zhang, Y., Chen, Y.S., Westerhoff, P., Crittenden, J., 2009. Impact of natural organic matter and divalent cations on the stability of aqueous nanoparticles. Water Res. 43, 4249–4257. https://doi.org/10.1016/j.watres.2009.06.005

Zhou, Y., Cheng, T., 2018. Influence of natural organic matter in porous media on fine particle transport. Sci. Total Environ. 627, 176–188. https://doi.org/10.1016/J.SCITOTENV.2018.01.210

Zhu, M., Wang, H.T., Keller, A.A., Wang, T., Li, F.T., 2014. The effect of humic acid on the aggregation of titanium dioxide nanoparticles under different pH and ionic strengths. Sci. Total Environ. 487, 375–380. https://doi.org/10.1016/j.scitotenv.2014.04.036